JCAMECH

Predicting Low Cycle Fatigue Life through Simulation of Crack in Cover Plate Welded Beam to Column Connections

Mehdi Ghassemieh[1,*,] Moein Rezapour[2], AshkanThaghinia[2]

[1]*Full Professor and corresponding author, College of Engineering, School of Civil Engineering, University of Tehran,*

Tehran, Iran

[2] *Graduate Student, College of Engineering, School of Civil Engineering, University of Tehran, Tehran, Iran*

Abstract

This paper presentsa low cycle fatigue life curve by simulating a crack in a cover plate welded moment connection. Initiation of ductile fracture in steel is controlled by growth and coalescence ofmicro-voids. This research useda numerical method using finite element modeling and simulation of ductile crack initiation by a micromechanical model. Therefore, a finite element model of a cover plate welded moment connection was developed in ABAQUS software, and a FORTRAN subroutine was used in order to simulate cracking in the connection model. Thus, each crack location and the number of cycles to initiate the crack weredetected. Utilizing cyclic void micromechanicalmodelofgrowth analysis, which is a technique to predict fracture in a ductile material, six different cover plate connections (divided in three categories) were modeled in the steel moment frame,and then their critical points to trigger the crack were identified. Finally, for the cover plate moment connection, considering the constant amplitude of loading curves data and in order to present the low cycle fatigue life prediction, displacement versus the number of half cycles diagram is produced.

Keywords: Low cycle fatigue, Cyclic void growth modeling, Cyclic loading, Cover plate moment connection.

1. Introduction

Accurate prediction of fracture is necessary and essential in many engineering applications and especially further developing fracture resistant design provisions for steel structures is critical for stuctural engineers. The Northridge earthquake occurred in the 1994 caused severe damages to many steel connections [1]. These brittle failureswere observed in many steel moment frame connections. Thus the need for further research to advance the ability to predict fracture model was noticed. Ductile fracture in metals occurs by the mechanism of void growth and coalescence. Ductile fracture initiates in fewer than twenty constant amplitude cyclesknown as ultra-low cycle fatigue (LCF) [2;3]. LCF with its extensive plasticity is related to the fracture mechanics and fatigue; which is an interaction between fracture and fatigue. Many connections may experience LCF, which results in fracture of the joint due to having the initial cracks being extended. Cracks can cause a low cycle fatigue failure; and also the damage accumulated during the next seismic excitation can cause the existing cracks to grow and run to a fracture in the joint [3;4].

Therefore, one needs to establish the safety of the structure when subjected to earthquake loading.

In practice, beams welded to column connections are typically inspected vitually during or after an earthquake. Many cracks can be detected, and some small cracks may not be found by visual inspections. Consequently, beside the inspection, one requires an analytical and/or a computational method in order to predict the detection of cracking in the connections. In recent years, the computational tools provided by the state-of-the-art computers, inspired the researchers to develop micromechanical models of ductile crack initiation. Among these models, stress modified critical strain model and void growth model are proposed for prediction of ductile crack initiation under monotonic loading conditions. Degraded significant plastic strain model and cyclic void growth model are also proposed for cyclic loading protocols. A comprehensive and detailed description of these models is presented by Kanvinde and Deierlein [5]. The aforementioned micromechanical models are used to predict ductile crack initiation in plates having bolt holes, plates having reduced sections, steel braces, and base plate connections with complete joint penetration [6]. Badrkhani and Ghassemieh investigated the effectiveness of reinforcing fillet welds in preventing cracking in the penetration welds and show that The aforementioned minimum size of the reinforcing fillet welds depends mainly on thickness of the column flange [7;8]. Lim et al. focused on the low cycle fatigue behavior of Tee stub as well as end plate moment connection by conducting full scale experimental tests and developing the model to predict the life cycle [9]. Amiri et al. proposed a method of simulating fracture in steel structures under large amplitude cyclic straining. The method was developed based on an existing micro-mechanical model for predicting crack initiation in ultra-low cycle fatigue [10]. They developed a step-by-step simulation of material degradation of column to base plate connection through the context of finite element method. Zhou et al. presented the seismic low-cycle fatigue assessment of welded beam to column connection in steel moment resisting frames using a general methodology [11]. Bai et al. proposed a model of crack initiation and propagation in steel connection subjected to ultralow cycle fatigue. Their model could be included in the general framework of lumped damage mechanics [12]. Liu et al. experimental investigated on a series of welded T-joints subjected cyclic loading to clarify their failure mechanisms in the ultra low cycle fatigue with a crack initiation at several cycles [13]. Fatigue deformability curves of several connection categories are developed using the available cyclic tests. On each connection of moment frame, inter storey drift history was imposed by seismic dynamic analysis. Based on Palmgren–Miner's rule and the

experimental date, fatigue damage calculation and fatigue prediction was carried out for the welded connection. Pereira et al. conducted an experimental study on the ultra low cycle fatigue behavior of S185 structural steel [14]. They also used the nonlinear finite element method of analysis to compute the history of relevent parameters of the investigated model.

Čermelj et al. proposed a phenomenological criterion for crack initiation based failure prediction of steel structural components subjected to cyclic loading [15]. They showed important difference in fatigue behavior between some joints. Liao et al. studied several welded connection specimens between the steel tube column and H-beam flange under monotonic loading [16]. Their results show when the fracture toughness parameters were changed about twenty percent, the predicted fracture result ranges were acceptable. Tong et al. investigate the fatigue failure behavior of experimental numerical by conducting on the six full scale beam-to-column welded joints [17]. They demonstrated the method based on continuum damage mechanics can successfully predict fracture behavior of beam-to-column welded joint with reasonable accuracy.

In this study, a micro-mechanical model is integrated into the finite-element program in order to simulate crack initiations in the cover plate welded beam to column connection. For this purpose, a Fortran code is linked with the ABAQUS software for simulating the crack and specifically to predict when and where the crack initiates. By understanding the crack initiation and the location of this crack, a trendline for low cycle fatigue under various constant drift angles are put together. The trendline provides a number of cycles for the crack to initiate by applying the specific drift angle.

2. Cyclic void growth modeling

The initiation of ductile fracture in steel materials is controlled by growth and coalescence of micro voids in their matrix structures. Rice in an analytical study demonstrated that a single spherical void in an elastic perfectly plastic continuum is promoted by a high-stress triaxiality ratio and the equivalent plastic strain. The stress triaxiality ratio is defined; as follows [4]:

$$T = \sigma_{mean} \big/ \sigma_{misses} \qquad (1)$$

in which σ_{mean} is the mean stress (or the hydrostatic stress) and σ_{misses} is the von Mises stress.

Kanvinde and Dierlein predict fracture when the equivalent plastic strain at any points exceeds a critical value; as follows [2;5]:

$$\varepsilon_p > \varepsilon_{p_{critical}} = \alpha \times e^{-1.5T} \qquad (2)$$

where α is the the parameter that quantifies the material resistance to fracture. The growth rate of the void radius is calculated by equation 3:

$$\frac{dR}{R} = C \times e^{1.5T} d\varepsilon_p \qquad (3)$$

In the above equation R is the void radius, c is a material parameter and $d\varepsilon_P$ is the incremental equvalent plastic strain; which can be calculated by the equation 4 [2]:

$$d\varepsilon_p = \sqrt{\frac{2}{3} d\varepsilon_p^{ij} \times d\varepsilon_p^{ij}} \qquad (4)$$

Kanvinde and Dierlein proposed the Cyclic Void Growth Model (CVGM) by extending the void growth model (VGM) [5]. They adopted the proposed model for ULCF loading. The CVGM is defined by two equations. The first equation imposes the fracture demands by developing the void growth index due to low cycle fatigue (cyclic loading) and the second one is about fracture toughness as presented by the critical void growth index. The first one is equation 5:

$$VGI_{cyclic} = \frac{\ln R/R_0}{c} = \sum_{tensile\ cycles} \int_{\varepsilon_1}^{\varepsilon_2} e^{|1.5T|} d\varepsilon_p$$
$$- \sum_{compressive\ cycles} \int_{\varepsilon_1}^{\varepsilon_2} e^{|1.5T|} d\varepsilon_p \qquad (5)$$

whereε_1 and ε_2 are the limits of integration corresponding to start and end of each cycle. The second one is equation 6 [5]:

$$VGI_{cyclic}^{critical} = VGI_{monotonic}^{critical} \times e^{-\lambda\varepsilon_p} \qquad (6)$$

where the equivalent plastic strain that has accumulated up to the beginning of each tensile excursion of loading, $VGI_{monotonic}^{critical}$ and λ are material parameters calibrated by material tests subjected to monotonic loading which determines the rate at which ductile fracture toughness degrades with respect to the damage.

In the above model the crack initiates when the following criterion takes place:

$$VGI_{cyclic} > VGI_{cyclic}^{critical} \qquad (7)$$

3. Investigated connections

Number of I-beam to box column connections with cover plates are designed in order to satisfy the provisions for the special steel moment frame structure. The connection consists of top and bottom cover plates; where the finger shaped top cover plate and rectangular bottom plate are groove welded to the column flange. Cover plates are connected to the beam flange with both longitudinal and transverse fillet welds.Continuity plates were located on both sides of the column web.

Six models are chosen from those designed connections and are modeled in ABAQUS software. Figure 1 and Table 1 present the geometrical dimensions of all the connections and their components. For being brief and due to vast data from the analyses, results of the model 1 (M1) are only presented in detail.

4. Finite element modeling

For all steel materials, Young's modulus is set equal to 200 GPa, and poisson ratio was considered as 0.3. For the nonlinear material properties, a combined isotropic and kinematic hardening model is adopted since the structure is mainly subjected to cyclic loading. Stress-strain relation input in the material model is presented in Table 2. The combined isotropic and kinematic hardening is based on Lemaitre's investigation [18]. In his model, the size of the yield surface (σ^0) is defined as a function of equivalent plastic strain (ε^{pl}), field variables (*f*) and temperature (*T*). This dependency can be modelled by an exponential law for materials subjected cyclic loading as following equation:

$$\sigma^0 = \sigma|_0 + Q_\infty[1 - \exp(-b\varepsilon^{pl})] \qquad (8)$$

Where $\sigma|_0$ is the yield surface size, and Q_∞ and *b* are additional material parametersand the evolution of the kinematic component of the model is defined:

$$\dot{\alpha} = C\bar{\dot{\varepsilon}}^{pl} \frac{1}{\sigma^0}(\sigma - \alpha) - \gamma\alpha\bar{\dot{\varepsilon}}^{pl} + \frac{1}{C}\alpha\dot{C} \qquad (9)$$

where*C* and γ are material parameters, $\dot{C}$ is the rate of change of *C* with respect to temperature and $\bar{\dot{\varepsilon}}^{pl}$ is the equivalent plastic strain. This evolution law defines the rate of α to be in the direction of the current radius vector from the center of the yield surface (σ - α). This equation is the basic Ziegler law, and the difference is that $\gamma\alpha\bar{\dot{\varepsilon}}^{pl}$ has been added. This parameter introduces the nonlinearity in the evolution law.
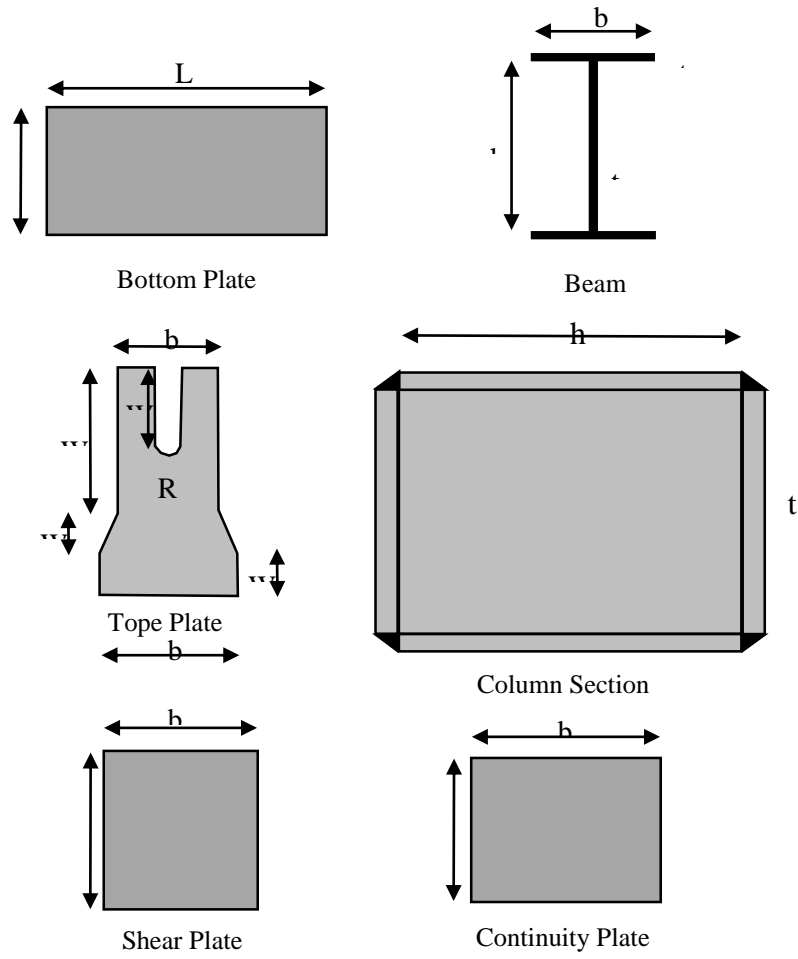
Figure 1. I-beam to box column connection geometry

Table 1.Connection Model Specimens (all dimensions are in cm)

			Connection type				
			M1	M2	M3	M4	M5	M6
I beam	bf	20	20	20	25	35	35
	tf	1.5	1.5	1.5	2	2	2
	hw	25	40	40	50	55	60
	tw	0.6	0.8	0.8	1	1	1
Column	h	30	35	35	45	55	60
	t	2	2.5	2.5	3	3	3
Continuity Plate	B	30	35	35	45	55	60
	t (top)	3.5	3.5	3.5	3	4	4
	t (bottom)	2	2	2	2	3	3
Shear Plate	b	10	10	10	10	10	10
	d	15	31	31	35	42	45
	t	0.8	0.8	0.8	1	1	1
Bot. Plate	a	23	26	23	29	39	40
	L	30	45	51	56	61	66
	t	2	2	2	2	3	3
Top Plate	w1	17	33	39	42	45	50
	w2	6	5	5	7	9	9
	w3	5	5	5	5	5	5
	w4	10	-	-	7	18	15
	b1	17	15	15	21	0	30
	b2	23	20	20	28	40	40
	t	3.5	3.5	3	3	4	4

Table 2. Material properties

yield stress (MPa)	plastic strain
244.70	0
278.48	0.02
301.05	0.04
318.36	0.06
332.57	0.08
344.69	0.1
355.32	0.12
364.81	0.14
373.40	0.16
381.27	0.18
388.53	0.2
388.53	0.3

Groove welds are modeled by tie constraints between nodes. Therefore, the connections between the top and bottom plate to the flange of column are modeled by tie constraints. The loading on the connection is controlled by displacement at the end of the beam. This loading is cyclic static and the protocol of that consists of only one displacement which is repeated as long as cracking occurs in the connection. Due to nonlinearity of the system, large displacement analysis in the software is considered.

A three-dimensional finite-element model of the connection is developed by ABAQUS general purpose finite-element software. The finite-element model consists of quadratic hexahedral elements that utilize reduced integration. Cover plates at the top and bottom of connections were modeled in ABAQUS software using C3D8 element; and every part meshed independently. Mesh with the incompatible modes is selected for the connection, and the final mesh converged for the analysis purposes is presented in Figure 2.

The boundary condition imposed on the FE model is presented in Figure 3. According to this figure, rotation is free at the both end of the column and displacement is subjected at the beam end.
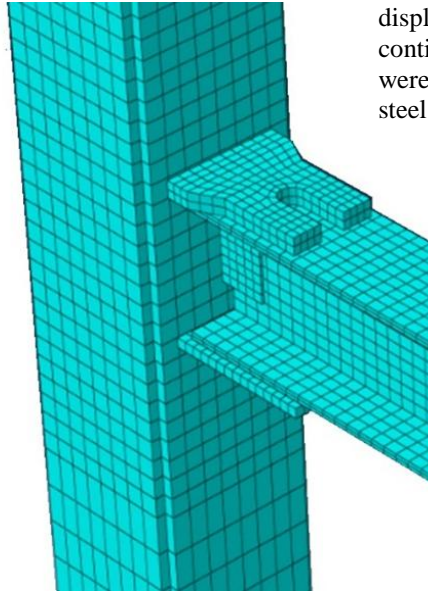
Figure 2. Finite element model of the connection

displacement of the beam tip. Beam, column, continuity plate and other parts of the connection were all ST37 steel material similar to ASTM A36 steel [21].

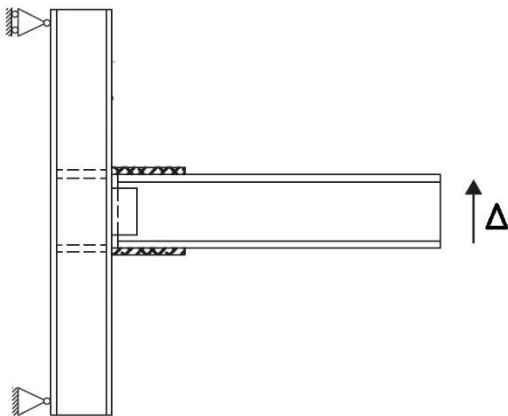**Figure 4. Test setup of the experimental program [19]**

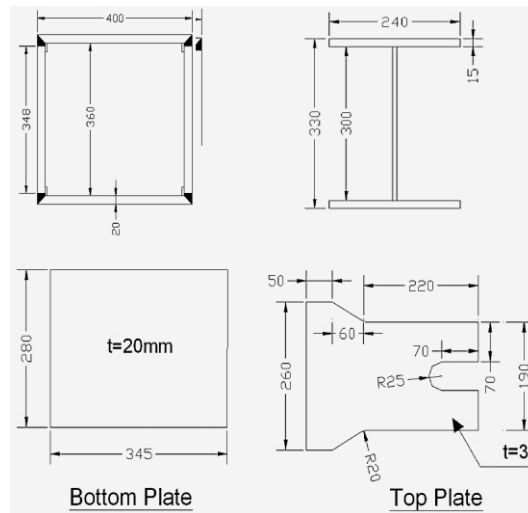Figure3. Boundary condition imposed on the model

Figure 5. Geometrical detailing of the cover plate connection

4.1 Finite element verifications

Results obtained from the experiments on the cover plate connections conducted by Sanee Nia et al. were used for the verification of the finite-element model [19]. The test setups along with the geometrical detail of one of the connections are illustrated in Figures 4 and 5. The experimental program covered the testing of many cover plate connections subjected to cyclic loading. As illustrated in the experimental setup, the column is placed horizontally, and the beam is set vertically. All specimens were subjected to slow rated cyclic loading at the tip of the cantilever beam based on AISC [20]; in which controlling parameter was the

The cyclic test of the connections is simulated by the finite-element program, and the results are presented. A close look at Figure 6 reveals that the analytical results being stiffness and strength are in good agreement with experimental results. The slight difference between analytical and experimental results can be mainly due to the uncertainties in the mechanical property of the test specimens, uncertainties of the mechanical modeling, and unavoidable residual stress. Now that the finite-element results are verified, cracking simulations of the connections subjected to low cycle fatigue utilizing the finite-element method is presented in the next section.
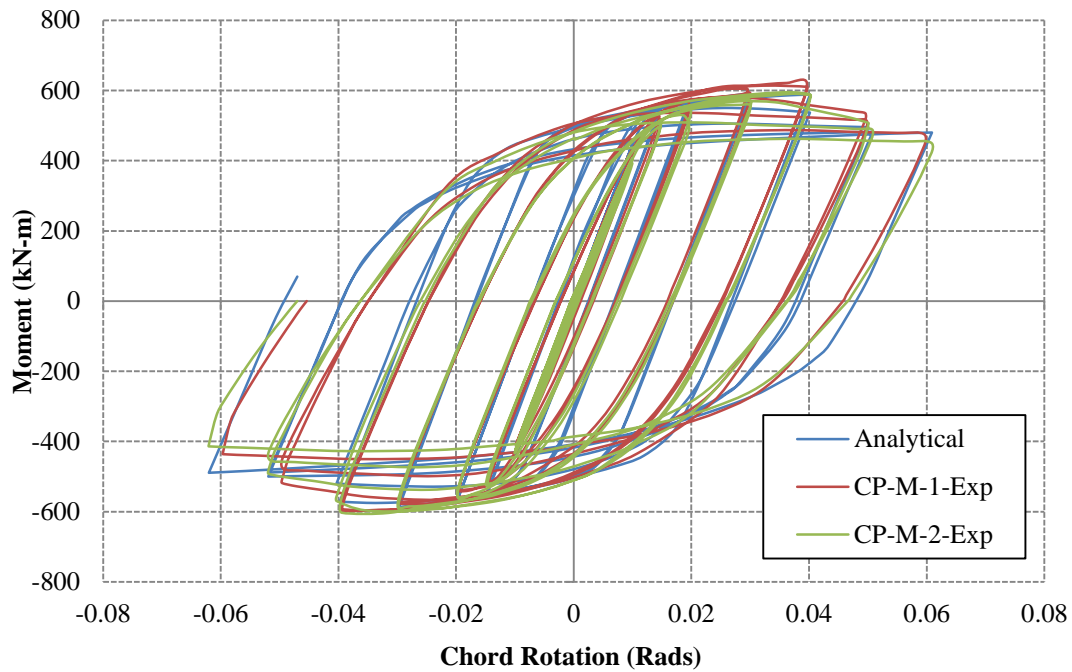
Figure 6. Verification of the Finite element results (cyclic moment rotation)

5. Cracking simulations for CVGM variables under constant amplitude drift angle

Cyclic void growth model (CVGM) is used to predict ductile fracture in the cover plate steel moment connections. Under ultra-low cycle fatigue utilized by constant amplitude drift angle, CVGM is adopted for simulating the crack initiation. Steel behavior under ultra-low cycle fatigue is similar to that of monotonic ductile fracture. The main difference is that LCF mechanism is accompanied by reduction in fracture resistance due to damage accumulation in material.

The M1-M6 connection model specimens presented in Table 1 are used for the cracking simulations in this study. A FORTRAN code is written specifically for this study to be linked with ABAQUS software in order to calculate the cyclic void growth model variables at different integration points of the elements. Flowchart of this subroutine is shown in Figure 7, where,*CVGI* is the cyclic void growth index, *CVGIcr* is the critical cyclic void growth index, T is the stress and *PEEQ* is the equivalent plastic strain.

The connections are loaded by constant amplitude drift of 0.03, 0.04, 0.05, 0.06 and 0.07 drift angle radian loading. Results for the cyclic void growth model variables are obtained and shown in the following figures. The location of the initiate crack is shown in the ABAQUS results. By having the variables parameters from ABAQUS, the number of cycles which the crack initiates is calculated. Here, the results of M1 connection specimen is presented in detail while summary of other connections are presented later.

5.1 Cracking simulations on the 0.03 radian drift angle

Figures 8 and 9, illustrate the von Mises stress contour and equivalent plastic strain of the M1 finite element model at the end of the finite element analysis; respectively. As shown, the location of the maximum stress as well as maximum equivalent plastic strain is under the top beam flange right after the top plate and in the plastic hinge zone.

Figure 10 presents the contour of void growth index due to cyclic loading (VGI_{cyclic}) with constant amplitude of 0.03 radian drift angle. Also in that figure, the point of maximumVGI_{cyclic}indicates the location of cracking predicted by the CVGM. As illustrated in the figure, the growth index demand due to cyclic loading at the aforementioned drift angle is controlled by the points near the beam flanges close to the vicinity of the connection cover plates.
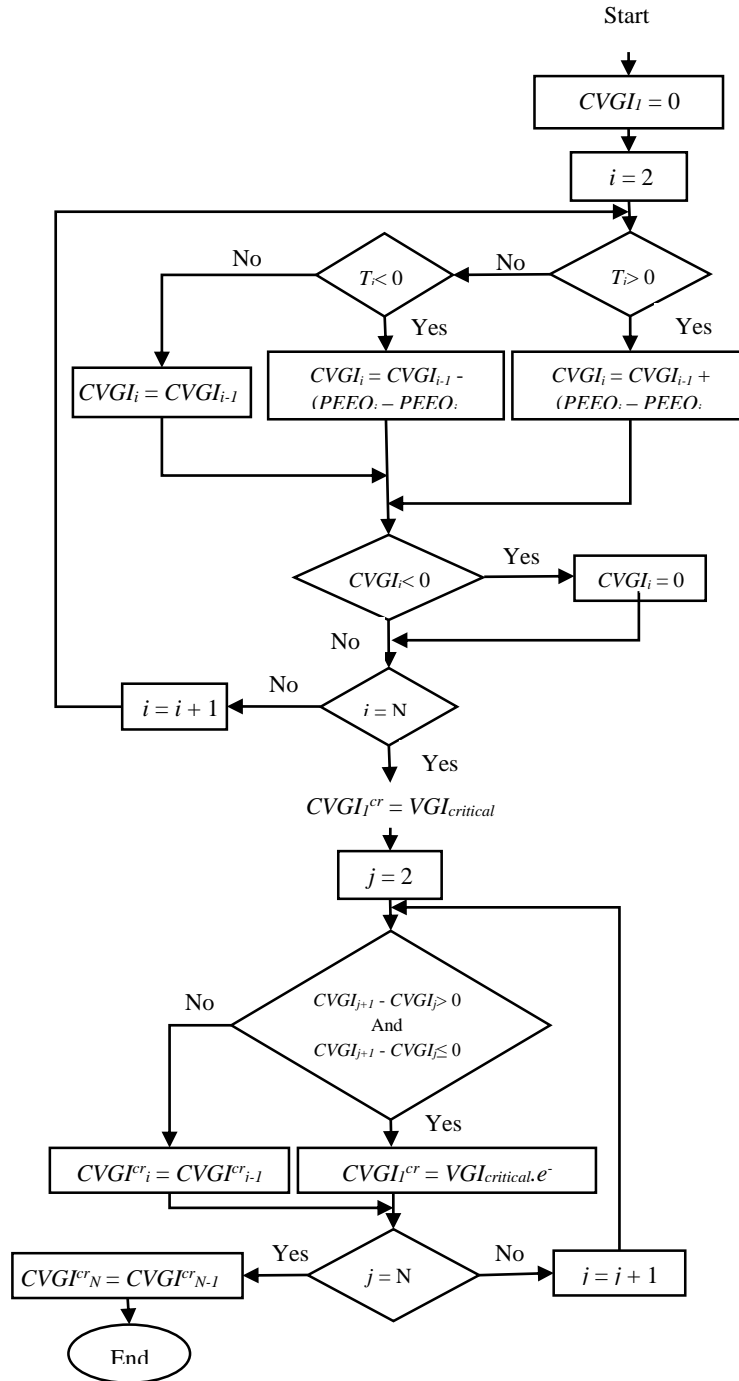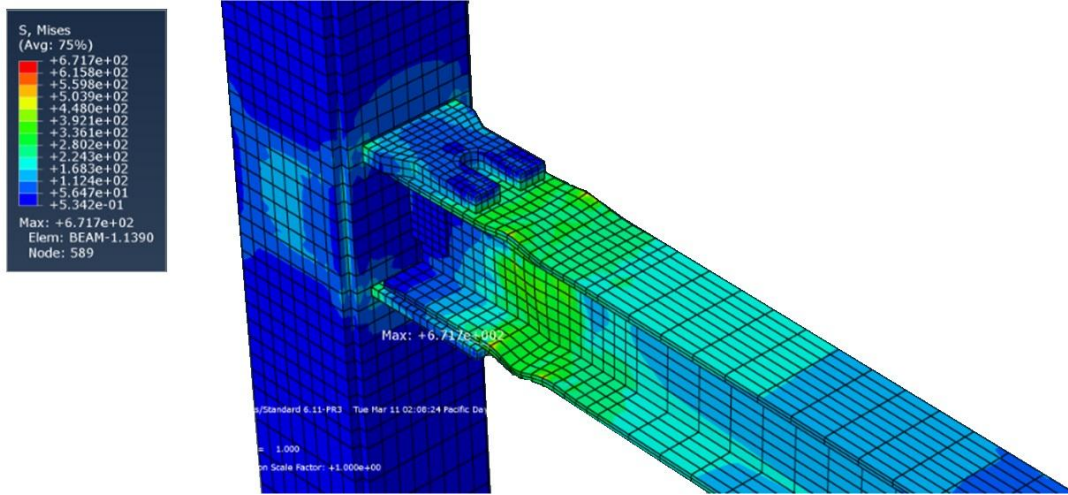
Figure 7 . Flowchart of the subroutine

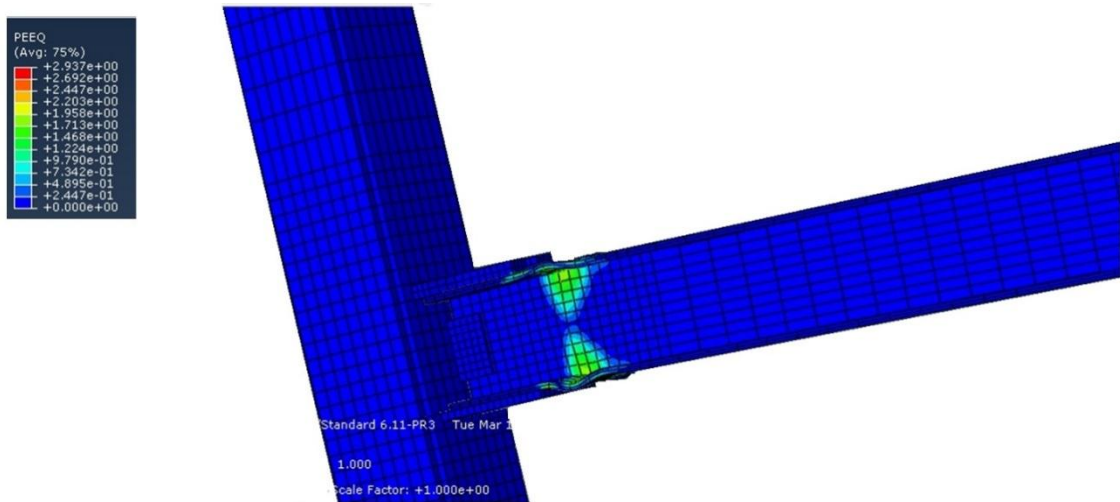**Figure 8. Contour of von Mises stress at the end of analysis (kg/cm²)**

Figure 9. Distribution of the equivalent plastic strain

Figure 11 illustrates the plots of cyclic growth index (*VGI_{cyclic}*)with the critical growth index and for the first element satisfying the condition of Eq. (7) in the finite element model. Intersection of the two curves indicates the satisfaction of the provision of Eq. (7) and therefore presenting the ductile crack initiation. As shown, one of the curves provides the fracture demand (presented in blue color) and the other one is resistance to the fracture (presented in red color). The crack initiation occurs when the demand exceeds the fracture resistance. By utilizing the time sequence as the loading in the computer software, number of cycles for this aim can be calculated. As presented in Figure 6, the number of half cycle that results in crack initiation is twenty five for this drift angle.

5.2 Cracking simulations on the 0.04 radian drift angle

Figure 12 illustrates the contour of the *VGI* for the 0.04 radian drift angle. As shown, again the

location of the crack initiation is under the top flange of the beam and immediately after top plate in the plastic hinge zone where the plastic strain has its maximum value.

As shown in Figure 13, again the intersection of two curves presents initiation of the crack. Considering the intersection of the two graphs in the figure, the half cycle for the initiate crack is fourteen for this drift angle.

5.3 Cracking simulations on the 0.05 radian drift angle

Figure 14 shows the location of the crack initiation which is under the bottom flange of the beam and precisely after bottom plate in the plastic hinge zone where the plastic strain has its maximum value. As presented in the Figure 15, the intersection of two curves illustrates the state of crack initiation. The number of half cycle for the crack to initiate is eleven for this drift angle.

5.4 Cracking simulations on the 0.06 rad. drift angle

Figure 16 illustrates the location of the crack initiation is top of the bottom flange of the beam and after bottom plate in the plastic hinge zone where the plastic strain has its maximum value. The crack initiation occurs when the number of half cycle is six for the 0.06 rad. drift angle (as shown in Figure 17).
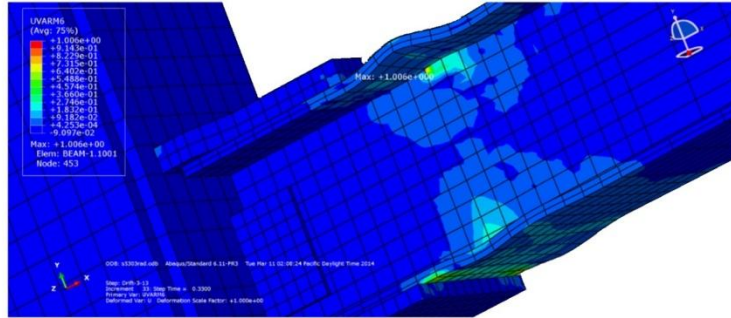

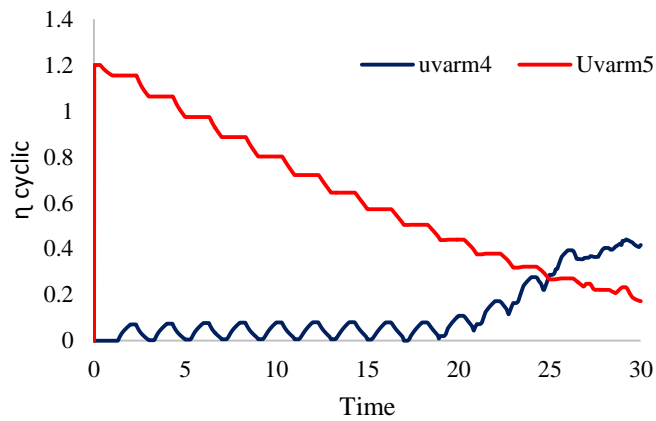**Figure 10. Contour of *VGI Cyclic* for the 0.03 radian drift angle**

Figure 11. *VGI* critical and *VGI* cyclic for the constant amplitude of 0.03 radian
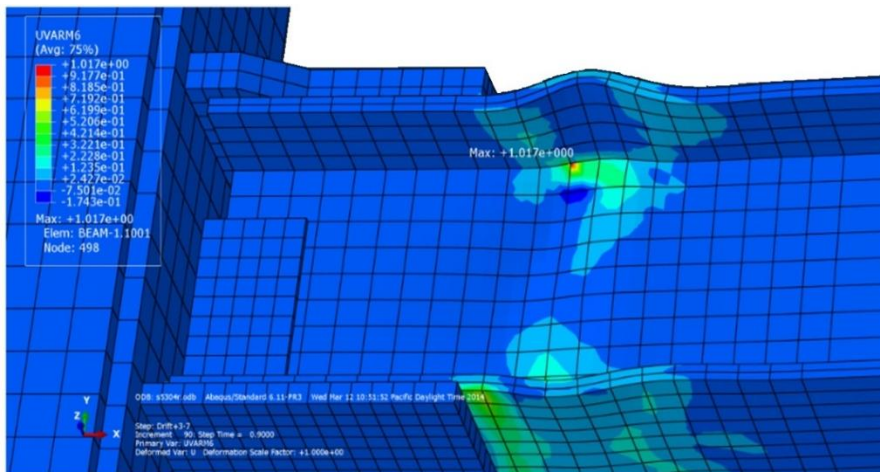

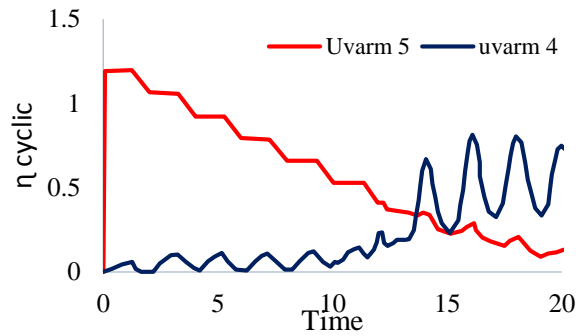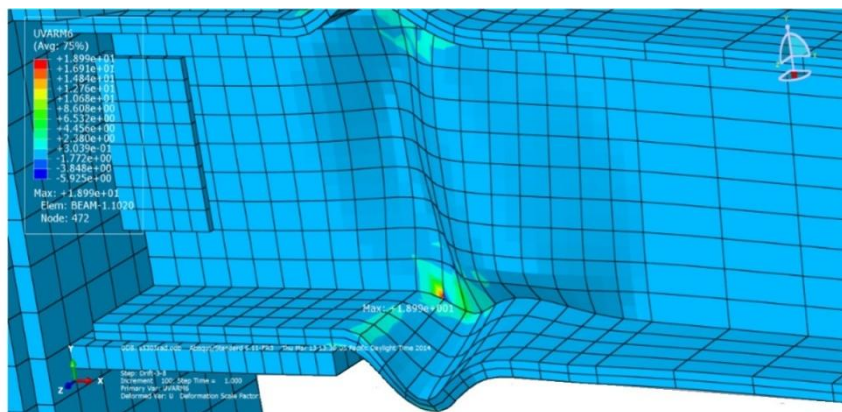**Figure 12. Contour of *VGI* Cyclic for the 0.04 radian drift angle**

Figure 13. *VGI* **critical and** *VGI* **cyclic for the constant amplitude 0.04 radian**

Figure 14. Contour of *VGI Cyclic* **for the 0.05 radian drift angle**
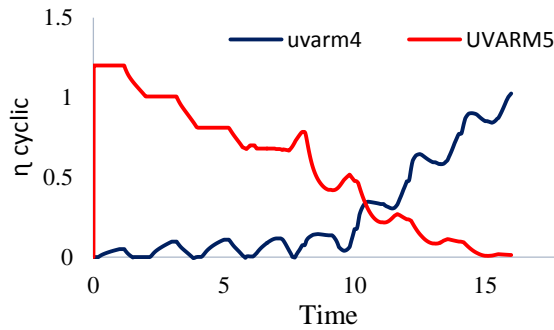

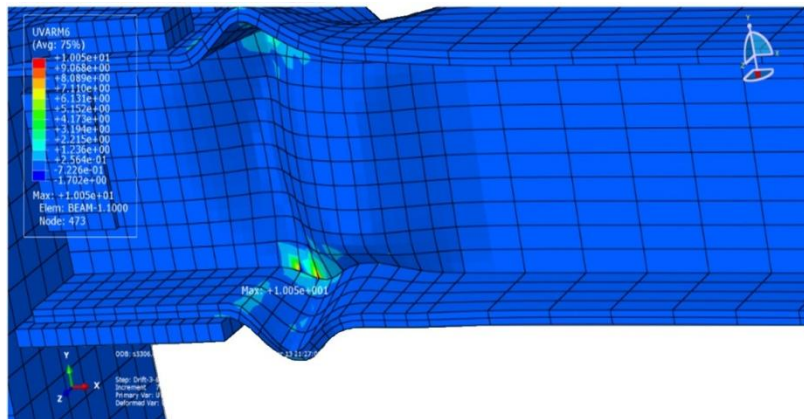**Figure 15.** *VGI* **critical and** *VGI* **cyclic for the constant amplitude 0.05 radian**

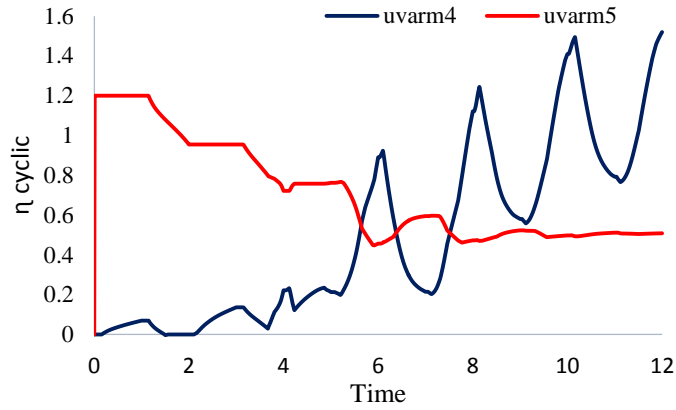**Figure 16. Cracking simulations on the 0.06 radian drift angle.**

Figure 17. *VGI* critical and *VGI* cyclic for the constant amplitude0.06 rad.

5.5 Cracking simulations on the 0.07 radian drift angle:

For this particular drift angle, the location of the initiate crack is under the top flange of the beam and

after top plate in the plastic hinge zone where the plastic strain has its maximum value (shown in Figure 18). Examining the growth index plots (Figure 19), the number of half cycle for the crack to initiate crack is four for this drift angle.
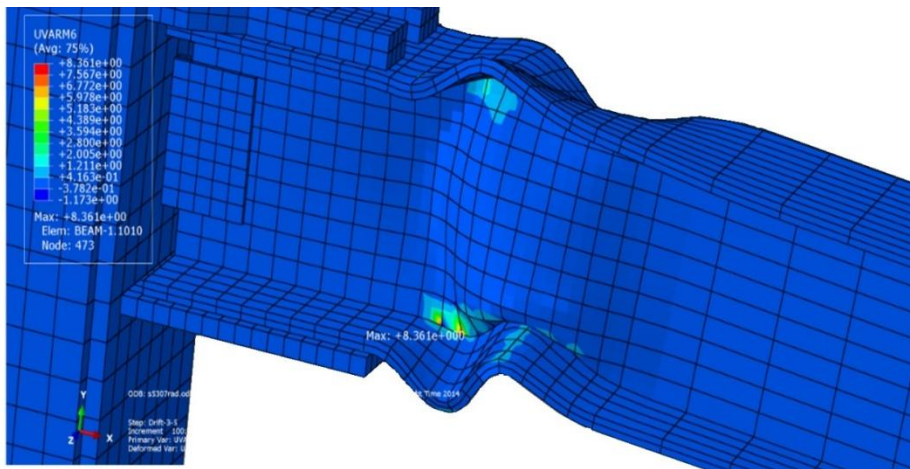

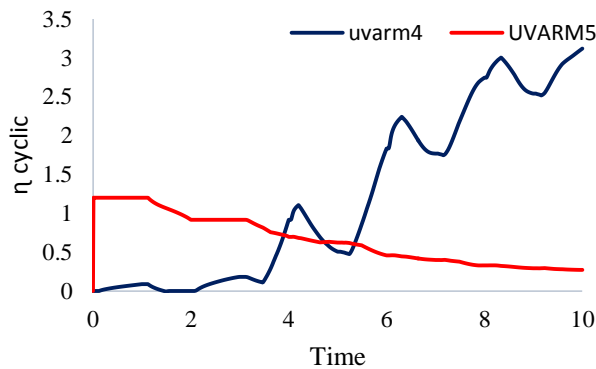**Figure 18. Cracking simulations on the 0.07 rad. drift angle**

Figure 19. *VGI* critical and *VGI* cyclic for the constant amplitude 0.07 radian.

In this study, the cracking parameters for six connections are presented and computed. The number of the half cycle in which cracking initiates is calculated by the growing cyclic loading on six model subjected under the constant amplitude. In table 3, results for six connection models subjected to different displacement amplitudes are presented. These results consist of the cycle numbers in which crack initiation are occurred for all models. According to the results obtained, the smaller the amplitude, the more cycle will be need to initiate the cracking.

Table 3. Number of cycles causes crack initiation for all Models (M1-M6)

Model	Amplitude loading (%)				
	0.03	0.04	0.05	0.06	0.07
M1	25	14	11	6	4
M2	32	17	15	13	9
M3	19	13	12	8	6
M4	17	10	8	6	4
M5	25	15	12	7	3
M6	25	16	11	6	5

The relation between the cycle number and the amplitude is not linear and can be proposed by Logarithmic function as illustrated in Figure 20 for M1. In this function, the concavity is upward and this means if the low displacement amplitude decreases slightly, the number of the half cycle will increase in more tangible.
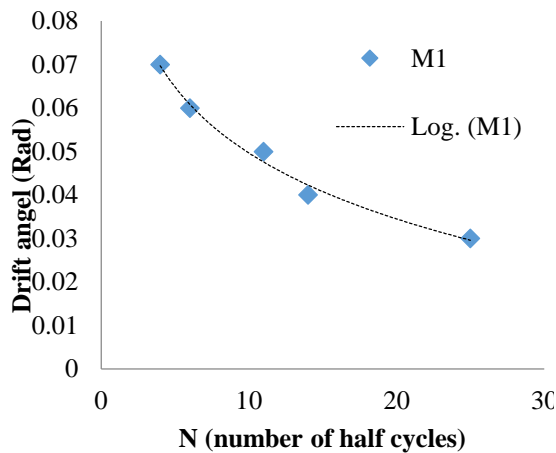

Figure 20. Drift-cycle curve of low cycle fatigue

Energy dissipation of these six models is one of the most important parameters, which determines the overall behavior of structure and decreases after initiation of cracking. In table 4, this parameter is indicated for six models before initiation of cracking. According to this table, the higher the amplitude, the more energy dissipation must be seen but because of the fewer cycles needed to initiate the cracking in the higher amplitude, the smaller the amplitude, the more energy dissipation is observed.

Table 4. Energy dissipation before initiation of cracking (kj)

Model	Amplitude loading (%)				
	0.03	0.04	0.05	0.06	0.07
M1	606	406	347	266	222
M2	1134	693	658	641	552
M3	1117	920	914	742	633
M4	1319	976	947	888	671
M5	2278	1622	1404	1252	681
M6	2340	1801	1523	1015	933

6. Conclusions

In this research, a numerical method is adopted using finite-element modeling and simulation of crack initiation by a micromechanical model. For this reason, a finiteelement model of a cover plate welded moment connection is developed in the ABAQUS software environment. A FORTRAN subroutine is implemented into the finite-element model in order to simulate cracking in the connection utilizing the cyclic void growth model. The adopted method provides results in terms of location and time of crack initiation in the cover plate welded moment connection. Then numbers of numerical specimens are subjected to the low cycle fatigue loading. Low cycle fatigue loading is applied by cyclic loading with several deferent amplitude intensities. For one model the cycles of initiate crack versus displacement curve is presented for ultralow cycle fatigue loading. By adopting this and having the displacement demand cycles can be predicted. For the six models which are divided to three types of connection cycles are shown, and it is investigated for the light connections; the stronger connection cycles for the initiate crack is bigger than smaller one. For the large drift angle such as 0.07 rad, the number of cycles are lower than nine cycles due to large plastic deformations. Results of the study show that the smaller the amplitude, the more cycle will be needed to initiate the cracking. Although higher rotation in the connection can make more energy dissipation, but the cracking occurs for the higher amplitudes in the fewer cycles. Because of the fewer cycles needed to initiate the cracking in the higher amplitude, the smaller the amplitude, the more energy dissipation is observed.

7. References

[1] Kaufmann, E., Fisher, J., Di. Julio, R., Gross, J., 1997, "Failure analysis of welded steel moment frames damaged in the Northridge earthquake". Gaithersburg, Md: NISTIR, 5944.

[2] Kanvinde, A. M., 2004, "Micromechanical simulation of earthquake-induced fracture in steel structures", Ph.D. Thesis, Stanford University.

[3] Iyama, J., Ricles, J. M., 2009, "Prediction of fatigue life of welded beam-to-column connections under earthquake loading". Journal of structural engineering, 135(12), pp. 1472-1480.

[4] Rice, J. R., Tracey, D. M., 1969, "On the ductile enlargement of voids in triaxial stress fields". Journal of the Mechanics and Physics of Solids, 17(3), pp. 201-217.

[5] Kanvinde, A., Deierlein, G., 2007 "Cyclic void growth model to assess ductile fracture initiation in structural steels due to ultra low cycle fatigue". Journal of engineering mechanics, 133(6), pp. 701-712.

[6] Fell, B. V., 2008, "Large-scale testing and simulation of earthquake-induced ultra low cycle fatigue in bracing members subjected to cyclic inelastic buckling". University of California.

[7] Ajaei,B., Ghassemieh, M., 2015, "Reinforcing fillet welds preventing cracks in partial joint penetration welds". International Journal of Steel Structures, 15(2), pp. 487-497.

[8] Ajaei, B., Ghassemieh, M., 2013, "Applicability of damage indices for detection of cracking in steel moment connections". Journal of Rehabilitation in Civil Engineering, 1(2), pp. 1-9.

[9] Lim, C., Choi, W., Sumner, E. A., 2012, "Low cycle fatigue life prediction using a four-bolt extended unstiffened end plate moment connection". Engineering Structures, 41, pp. 373-384.

[10] Amiri, H., Aghakouchak, A., Shahbeyk, S., Engelhardt, M., 2013, "Finite element simulation of ultra low cycle fatigue cracking in steel structures". Journal of Constructional Steel Research, 89, pp. 175-184.

[11] Zhou, H., Wang, Y., Yang, L., Shi, Y., 2014, "Seismic low-cycle fatigue evaluation of welded beam-to-column connections in steel moment frames through global–local analysis". International Journal of Fatigue, 64, pp. 97-113.

[12] Bai, Y., Kurata, M., Flórez-López, J. and Nakashima, M., 2016. "Macro-modeling of Crack Damage in Steel Beams Subjected to Nonstationary Low Cycle Fatigue". Journal of Structural Engineering, 142(10), p.04016076.

[13] Liu, Y., Jia, L.J., Ge, H., Kato, T. and Ikai, T., 2017. "Ductile-fatigue transition fracture mode of welded T-joints under quasi-static cyclic large plastic strain loading". Engineering Fracture Mechanics, 176, pp.38-60.

[14] Pereira, J., de Jesus, A., Xavier, J., Fernandes, A., 2014, "Ultra low-cycle fatigue behavior of a structural steel". Engineering Structures, 60, pp. 214-222.

[15] Ermelj, B., Moe, P., Sinur, F., 2016, "On the prediction of low-cycle fatigue in steel welded beam-to-column joints". Journal of Constructional Steel Research, 117, pp. 49-63.

[16] Liao, F., Wang, W., Chen, Y., 2015, "Ductile fracture prediction for welded steel connections under monotonic loading based on micromechanical fracture criteria". Engineering Structures, 94, pp. 16-28.

[17] Tong, L., Huang, X., Zhou, F., Chen, Y., 2016, "Experimental and numerical investigations on extremely-low-cycle fatigue fracture behavior of steel welded joints". Journal of Constructional Steel Research, 119, pp. 98-112.

[18] Lemaitre, J.,Chaboche, L., 1990, "Mechanics of Solid Materials", Cambridge University Press.

[19] Nia, Z. S., Mazroi, A., Ghassemieh, M., 2014, "Cyclic performance of flange-plate connection to box column with finger shaped plate". Journal of Constructional Steel Research, 101, pp. 207-223.

[20] AISC., 2005, AISC 341-05. "Seismic provisions for structural steel buildings". Chicago (IL): American Institute of Steel Construction.

[21] Correa, S. R., de Campos, M. F., Marcelo, C., de Castro, J. A., Fonseca, M. C., Chuvas, T., Padovese, L. R., 2016, "Evaluation of Residual Stresses in Welded ASTM A36 Structural Steel by Metal Active Gas (MAG) Welding Process". Paper presented at the Materials Science Forum.2.3023